Coincidence analyzing-power measurements of the reaction $^{12}C(\vec{p},p'\gamma)^{12}C^*$ through the 15.11-MeV state

C. R. Lyndon, H. O. Funsten, C. F. Perdrisat, V. Punjabi, and J. M. Finn
Department of Physics, The College of William and Mary, Williamsburg, Virginia 23185

B. J. Lieb
Department of Physics, George Mason University, Fairfax, Virginia 22030

C. E. Stronach and N. L. Fuqua
Department of Physics, Virginia State University, Petersburg, Virginia 23803

H. S. Plendl, J. R. Mackenzie, and R. Nair
Department of Physics, Florida State University, Tallahassee, Florida 32306

J. R. Comfort and R. A. Giannelli
Department of Physics, Arizona State University, Tempe, Arizona 85287

J. J. Reidy and L. Redmond
Department of Physics, University of Mississippi, University, Mississippi 38677

P. E. Koehler and S. A. Wender
Los Alamos National Laboratory, Los Alamos, New Mexico 87545
(Received 31 October 1990; revised manuscript received 3 July 1991)

Coincidence analyzing-power measurements or asymmetries A_x^{coinc}, A_y^{coinc}, and A_z^{coinc} are presented for the $^{12}C(\vec{p},p'\gamma)^{12}C^*$ (15.11 MeV) reaction. A polarized proton beam at 318 MeV was used and data were obtained for three mutually perpendicular directions of polarization. A scintillator hodoscope was used for detecting scattered protons and four BGO detectors for the 15.11-MeV γ rays. Data are presented for eight azimuthal directions of the scattered protons around the beam direction, and for the polar angles averaged between 3.3° and 11.2°. The data are compared with both nonrelativistic and relativistic calculations. The average size of the asymmetries measured is somewhat less than both predictions and the results do not agree clearly with either prediction.

PACS number(s): 25.40.Ep, 24.70.+s

I. INTRODUCTION

There have been numerous comparisons in recent years of relativistic versus nonrelativistic treatments of the spin behavior of proton scattering on nuclei. The first comparisons of elastic proton analyzing powers, A_y, with distorted-wave relativistic impulse approximation (DRIA) calculations showed remarkable agreement, although nonrelativistic distorted-wave Born-approximation (DWBA) calculations gave approximate agreement [1].

As calculations of inelastic analyzing powers have become available, the picture that has so far emerged is not as clear-cut as in the elastic case. In the case of some transitions, such as for low-lying natural-parity states in even-even nuclei (^{24}Mg and ^{28}Si), relativistic distorted-wave calculations still gave excellent agreement [2] and, on the whole, relativistic calculations have tended to give somewhat better results than nonrelativistic calculations. But for some other states, microscopic DWBA calculations have done as well as or better than their relativistic counterparts, or neither has been able to fit the data well. For instance, relativistic A_y calculations for the 5^-(4.49-MeV) state of ^{40}Ca at E_p=362 MeV only fit the data out to a $\theta_{c.m.}$ of 20°, whereas a nonrelativistic DWBA calculation (using the Love-Franey NN interaction) does better beyond that point (although still not with very good agreement) [3].

In the case of ^{12}C, the target investigated in this experiment, the situation is particularly unclear. Neither type of calculation of A_y, the analyzing power, for natural-parity states shows good agreement with the data for scattering angles beyond the first minimum [2,4,5]. Two transitions to unnatural-parity states involving spin-flip have been studied so far at intermediate energies. In the case of the 12.71-MeV $J^\pi,T = 1^+,0$ state, a nonrelativistic distorted-wave calculation of A_y does somewhat better than a relativistic treatment at 400 MeV [6]; for 200-MeV data, a relativistic calculation with explicit treatment of exchange between the projectile and target nucleons does worse than another relativistic calculation

that does not include exchange terms in the transition amplitude [5]. The situation is similar for the 15.11-MeV $J^{\pi},T = 1^{+},1$ state. The nonrelativistic calculation makes predictions similar to the nonexchange relativistic calculation for A_y, and these fit the data better than a relativistic calculation with exchange included, although the latter does a better job with the unpolarized differential cross sections [4,5]. Measurements of $P - A_y$ (polarization minus analyzing power) for these two states at 400 MeV do not clearly favor either type of model [6].

The present experiment, a $(\vec{p},p'\gamma)$ coincidence study of the 15.11-MeV state, was undertaken to obtain more information to test the various reaction models since it probes bilinear combinations of inelastic amplitudes that are not accessible to $(\vec{p},p')$ experiments [7]. There has been one previous $(\vec{p},p'\gamma)$ measurement of the 15.11-MeV ^{12}C state. It was done using a magnetic spectrometer and BGO detectors with incident 400-MeV protons polarized normal to the p-p' plane by Hicks *et al.* [8,9]. They found evidence in favor of relativistic treatments, although not with complete agreement. The present experiment used incident 318-MeV protons at the external proton beam (EPB) of the Clinton P. Anderson Meson Physics Facility (LAMPF) polarized in turn along each of three mutually perpendicular directions. A plastic scintillator hodoscope detected protons scattered into a forward cone about the incident beam direction. Detection of the 15.11-MeV γ rays from the ground-state transition (branching ratio 88%) was by a group of four bismuth germanate (BGO) detectors which also served to identify the reaction.

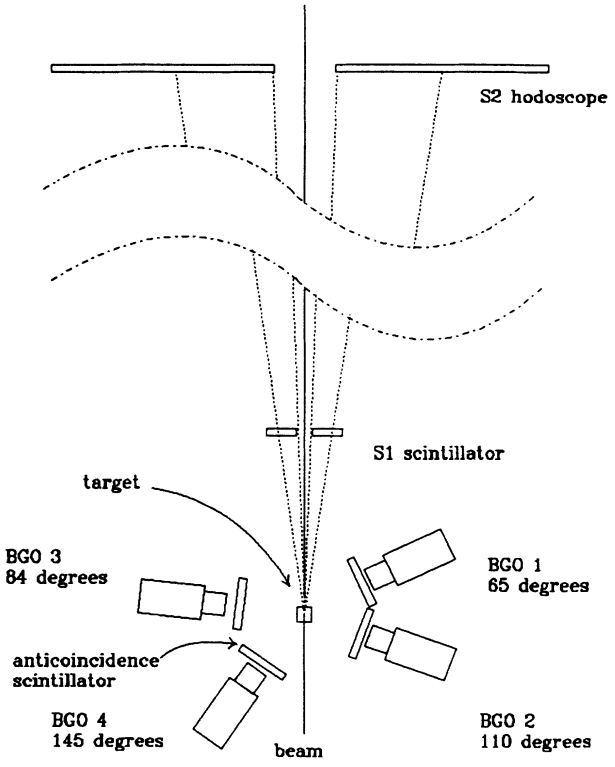

FIG. 1. Schematic plan of the experimental apparatus.

II. EXPERIMENTAL SETUP

Scattered protons were detected by means of a plastic scintillator hodoscope S2 located downstream of the target (see Fig. 1), operated in coincidence with a plastic scintillator S1 located between the target and S2. S1 was a 20-cm-diameter circular scintillator 46 cm downstream of the target centered around the beam with a 4-cm-diameter hole in its center to allow the beam to pass through. The singles rate in S1 was about 2 MHz. S2, also centered around the beam with a hole at its center, was located 230 cm downstream of the target and was made up of eight sector-shaped plastic scintillators overlapped to provide sixteen azimuthal angle elements of 22.5° each (see Fig. 2). The rates in the individual sector scintillators were 200–300 kHz. In front of the S2 sector-shaped scintillators were three overlapping ring scintillators (Fig. 3), designed to bin the scattered proton polar angle in 2° intervals. Because of the need for better statistics, the final data were summed over the polar angle bins. The bins were used for two corrections described below (a Doppler correction on the BGO energy spectrum and a light travel-time correction on S2·S1 timing spectra), and to monitor beam current. S1 and S2 detected protons scattered between laboratory polar angles of 3.3° to 11.2°, and had a resulting solid angle of 110 msr.

15.11-MeV γ's were detected by an array of four BGO detectors arranged in a horizontal plane around the target (Fig. 1). Each BGO detector was a 7.6-cm-diameter by 7.6-cm-long crystal and had a plastic anticoincidence scintillator in front of it to detect and veto charged particles. The singles rates in the BGO's (as vetoed by the anticoincidence scintillators) ranged from 5 to 16 kHz. Table I gives the angles for the BGO axes, distances from the target center to the BGO front faces, and BGO solid angles.

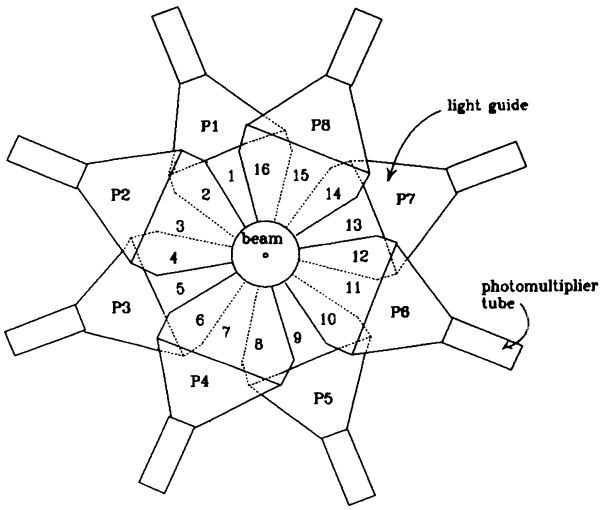

FIG. 2. Schematic front view of hodoscope array S2.

TABLE I. BGO angles relative to beam direction, distances from the front face to the target center, and solid angles.

	Normal and sideways			Longitudinal		
BGO	Angle (deg)	Distance (cm)	Solid angle (msr)	Angle (deg)	Distance (cm)	Solid angle (msr)
1	69	20.0	111	65	22.1	92
2	117	20.0	111	110	21.4	97
3	89	21.7	94	84	21.0	101
4	131	21.4	97	145	24.1	77

Since a magnetic spectrometer was not used for proton detection, the experiment was designed to identify an inelastic proton reaction exciting the 15.11-MeV state by detection of its ground-state γ transition in the BGO detector. The 15.11-MeV state lies near the 15.96-MeV proton separation energy in ^{12}C, and there are no higher bound levels in ^{12}C that can γ decay to the 15.11-MeV state. Hence a 15.11-MeV photon accompanied by an S1·S2 coincidence event uniquely identifies an inelastic proton scattered to the 15.11-MeV state. However, secondary reactions in the target can also excite the 15.11-MeV state, although 15.11 MeV is above the 10-MeV mean energy level of secondary evaporation neutrons. A calculation based on the total ^{12}C cross section of 288 mb [10] for scattering of 318-MeV protons and a target thickness of $\tau = 0.57$ cm showed secondaries contamination of 15.11-MeV γ's was less than 2.5%. Additionally, two measurements indicate that secondary interactions are not significant. First, the coincident amount of 15.11-MeV γ's scaled linearly with target thickness τ, and not with τ^2, as would be the case for secondaries. Secondly, the 15.11-MeV peak did not appear in the BGO energy spectrum for events to the right of the timing cuts in Fig. 4 (i.e., events with slower time of flight between S2 and S1 indicative of multinucleon target knock-out).

To compute the coincidence analyzing powers the polarization of the incident beam and the beam current were also monitored. The beam polarization P varied between 0.70 and 0.85. The beam polarization direction changed by 180° every two minutes. P had the same magnitude to within 2% for both directions of each polarization [11]. It was monitored by a LAMPF beam-line polarimeter, which determined the polarization from p-p scattering on a CH_2 target of known analyzing power. The beam current was kept low, ranging from 1 to 10 pA, in order to hold random BGO coincidences to about a 25% level, and was monitored in a LAMPF ion chamber and by the scintillators. The accelerator duty factor was 3%.

The main event trigger consisted of a coincidence between S1, one or more of the sector scintillators of S2, and a BGO vetoed by its anticoincidence scintillator. The output from each S2 sector scintillator and from S1 was fed into an ADC and, for the S2 sectors, the stop

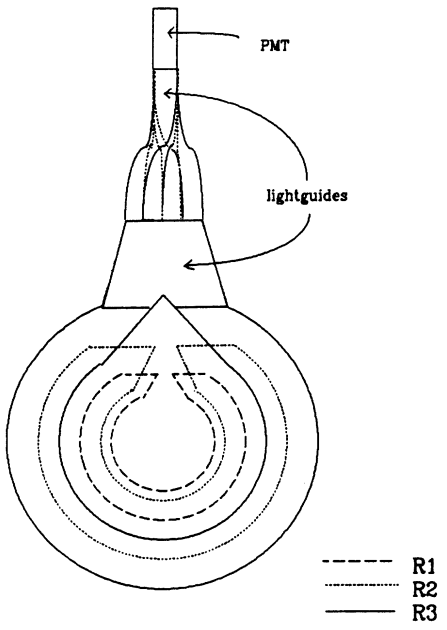

FIG. 3. Schematic front view of ring detectors.

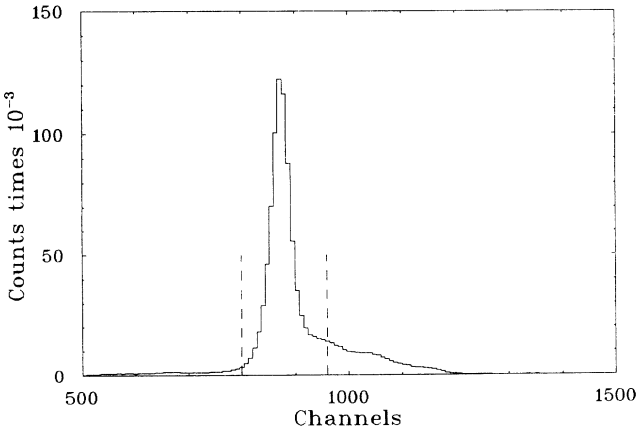

FIG. 4. Timing spectrum between one of the S2 sectors and S1. The width of the timing cut is 8 ns.

of a TDC. The start of the TDC's was S1. Similarly, each BGO was fed into an ADC and a TDC, with S1 again being the BGO TDC start. A bit register recorded which sectors, rings, BGO's and anticoincidence scintillators fired on each event, and also the polarization state of the beam. Besides the main event trigger, three other triggers were used: (1) a prescaled S1·S2 "singles" trigger was recorded, (2) a BGO "singles" trigger, and (3) a scaler event recorded the scalers of the BGO's, all the scintillators, a 1-MHz clock and the cumulative charge of the beam current ion chamber. Selected scalers were recorded both gated and ungated by "computer busy," to monitor dead time.

III. DATA ANALYSIS

Timing spectra between the various sector scintillators of S2 and S1 showed a main peak with a width dominated by the timing resolution of the apparatus (see Fig. 4). The timing spectra were corrected for light travel time in the sector scintillators, using information from the ring detectors. The timing resolution $\Delta t = 2$ ns (FWHM) corresponds to a ΔE in the scattered proton of 136 MeV (FWHM). This permitted discrimination against slower events on the right side of the cuts involving the knock-out of more than one nucleon in the target.

The pulse-height spectra from the sector scintillators of S2 are strongly correlated with S1·S2 timing; hence no cuts on the pulse height were employed. (Besides events eliminated by a timing cut, a pulse-height cut might have eliminated a few events that fell within the timing cuts but had unusually large pulse heights, but the number of these events corresponded roughly to the expected number of events with nuclear reactions in the sector scintillators. Since these events were still good for the purposes of the experiment, no cut on pulse height was used.)

The BGO spectra were energy corrected for two effects: (1) the γ-ray Doppler shift due to nuclear recoil was determined from the proton scattering direction given by S2; (2) variations in BGO pulse-height response due to daily ambient temperature changes in the EPB area of LAMPF were compensated in software event reconstruction, based upon 15.11-MeV peak centroid determination over intervals of a few hours.

Timing spectra between each BGO and S1 were used to eliminate random coincidences. The peak-to-valley ratio of a typical BGO timing spectrum was about 4:1. Figure 5 shows a BGO timing spectrum with the on-time and off-time cuts. The randoms component of the BGO spectrum was removed in the following manner. The off-time BGO energy spectrum [Fig. 6(b)], scaled by the ratio of the widths of the on-time to off-time BGO timing cuts, i.e., multiplied by

$$w = \frac{\Delta_{\text{on}}}{\Delta_{\text{off1}} + \Delta_{\text{off2}}} \tag{1}$$

(see Fig. 5), was subtracted from the on-time spectrum [Fig. 6(a)], to produce a randoms-subtracted on-time energy spectrum [Fig. 6(c)]. (The lower ends of these energy spectra, below 6 MeV, have been prescaled to reduce the domination of the 4.44-MeV peak.) To minimize bias-

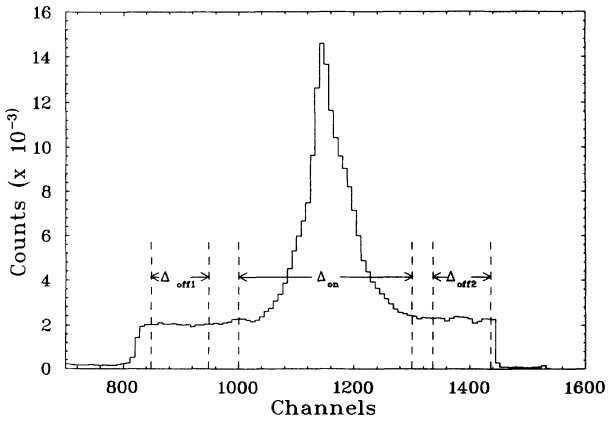

FIG. 5. Timing spectrum between a BGO and S1, with both on-time and off-time cuts shown. The on-time cut is three accelerator beam micropulse widths, and the off-time cuts are each one beam micropulse width.

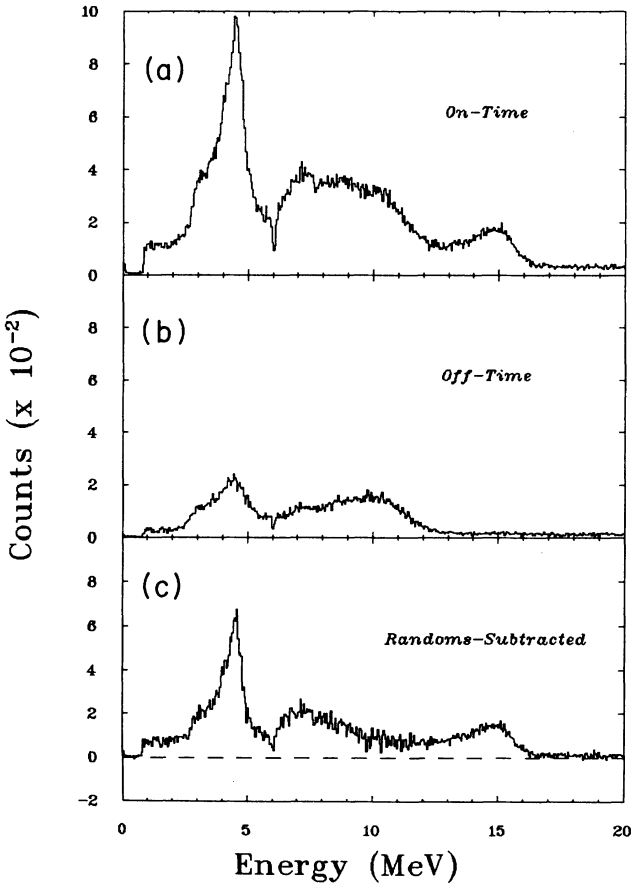

FIG. 6. On-time, off-time, and randoms-subtracted BGO spectra. These spectra have been corrected for temperature and Doppler shifts as described in the text. The lower end of each spectrum (below about 6 MeV) has been prescaled by one tenth.

ing due to location of the timing cuts in relation to the beam microstructure (every 5 ns), the widths of both the on-time and off-time cuts (Fig. 5) were chosen to be in integral numbers of beam micropulse widths.

The resulting randoms-subtracted spectrum shows the 15.11-MeV peak above a monotonically decreasing background [Fig. 6(c)]. This spectrum was then modeled by the following procedure. A calculated shape for the 15.11-MeV peak of centroid C and height H was obtained by an EGS4 [12] simulation of the BGO response to incident 15.11-MeV γ's. This peak shape was convoluted with a Gaussian of width W to account for the BGO energy resolution and added to an exponential background of the form $a(e^{-bx}+c)$. (It was found that an exponential background gave a lower χ^2 than a quadratic polynomial ax^2+bx+c background.) For each BGO, C and W were determined from a six-parameter fit (varying C, H, W, and the background parameters a, b, and c) to the randoms-subtracted spectra, summed over all S2 sectors and both directions of polarization $\uparrow$ and $\downarrow$. With the centroid position C and width W fixed at the values thus determined, the background parameters b and c were determined from a four-parameter fit (H, a, b, and c) to the BGO energy spectrum for combinations

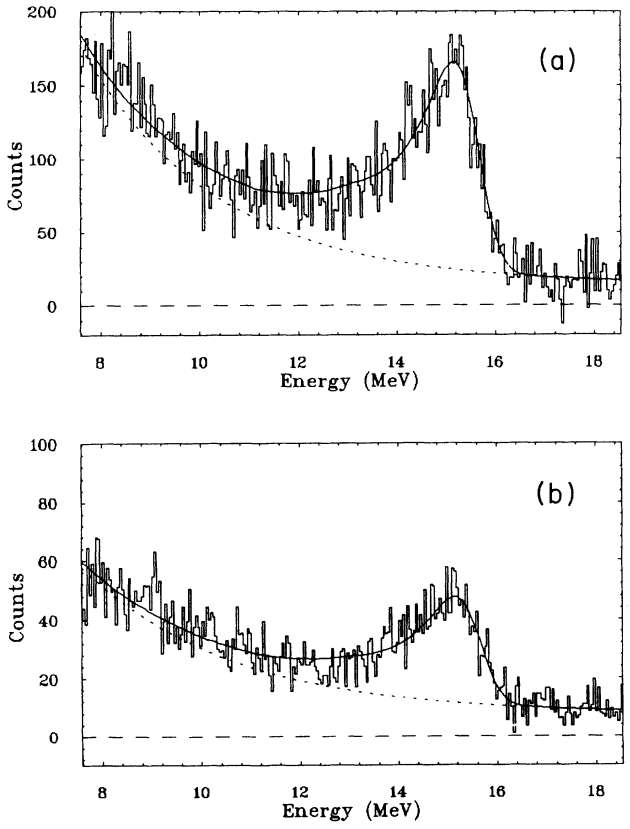

FIG. 7. The top spectrum and six-parameter fit are for data summed over all azimuthal proton directions and both directions of incident proton polarization. The lower spectrum and four-parameter fit are for a single azimuthal direction and both polarization directions. The on-time background is shown as a dotted line.

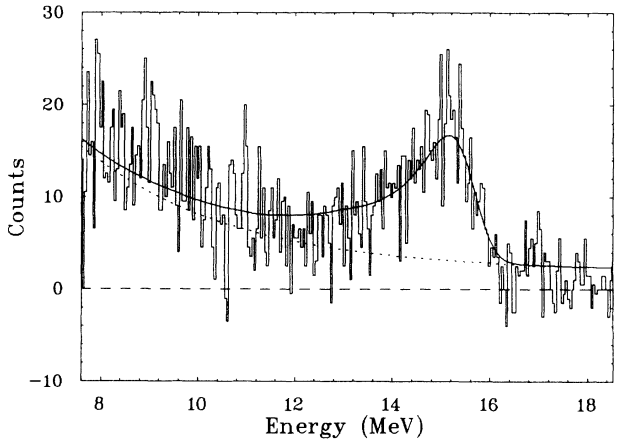

FIG. 8. Two-parameter fit corresponding to Fig. 7. The on-time background is shown as a dotted line.

of three azimuthal S2 sectors (see Sec. IV), combining $\uparrow$ and $\downarrow$ polarization data. Finally, with b and c fixed at the values thus determined, H and a were determined from fits to the spectrum for each combination of three S2 sectors and each direction of polarization ($\uparrow$ and $\downarrow$). The values of $H_\uparrow$ and $H_\downarrow$ from these final fits were used to compute the coincidence analyzing powers. A sample of data and a six-parameter fit are shown in Fig. 7(a), and a four-parameter fit for normal polarization scattering to the right is shown in Fig. 7(b). Figure 8 shows the final two-parameter fit corresponding to Fig. 7.

As a check, the method outlined above was used to fit data taken using 4.44-MeV γ's from a PuBe source located at the target position (with beam off). The above procedure resulted in a good fit to the calibration data, shown in Fig. 9.

The statistical errors in the heights H were evaluated by the CERN fitting routine HFIT [13], using as inputs the statistical errors from the randoms-subtracted BGO energy spectra, which were propagated from the errors

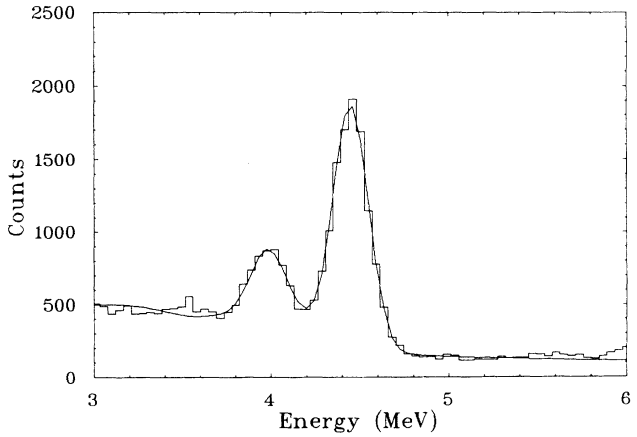

FIG. 9. Fit of 4.44-MeV source calibration spectrum with EGS4 spectrum convoluted with a Gaussian and added to the background function $a(e^{-bx}+c)$.

in the on-time and off-time energy spectra.

As discussed below, analyzing-power measurement errors reflect errors in the average incident beam polarization over each run and Q, the ratio of $\uparrow$ to $\downarrow$ beam charge. The errors in the average incident beam polarization (based on hourly measurements provided by LAMPF) were negligible compared to the uncertainties in H and Q. Q was monitored by both the ion chamber and scalers for selected S2 sector and ring scintillators. However, the behavior of the ion chamber system was found to be erratic and so it was not used in computing the analyzing powers. Instead, the scalers for S2 sectors and rings were selected to monitor Q in combinations which were polarization insensitive because of parity constraints. For normal polarization five quantities were used: the sums of the scalers P1+P8 (see Fig. 2), P4+P5, and the scalers for the three ring detectors. Q was evaluated for each of these five and the overall average was used in computing the analyzing powers. For sideways beam polarization the sums of P2+P3 and P6 +P7 were used. For longitudinal polarization the scalers for each of the paddles P1 through P8 and for the three ring detectors were used.

IV. RESULTS AND CONCLUSION

The measured quantities $H_\uparrow$ and $H_\downarrow$ were used to evaluate the γ-ray coincidence analyzing powers A_y^{coinc}, A_x^{coinc}, A_z^{coinc} defined as

$$A_i^{\text{coinc}}(\phi_p,\theta_\gamma,\phi_\gamma)=\frac{d^2\sigma/d\Omega_\gamma d\Omega_p(\phi_p,\theta_\gamma,\phi_\gamma)_\uparrow - d^2\sigma/d\Omega_\gamma d\Omega_p(\phi_p,\theta_\gamma,\phi_\gamma)_\downarrow}{P[d^2\sigma/d\Omega_\gamma d\Omega_p(\phi_p,\theta_\gamma,\phi_\gamma)_\uparrow + d^2\sigma/d\Omega_\gamma d\Omega_p(\phi_p,\theta_\gamma,\phi_\gamma)_\downarrow]},\quad i=x,y,z, \tag{2}$$

where x, y, and z are the three perpendicular directions of incident proton polarization P: y normal (vertical), x sideways (horizontal and perpendicular to the beam), and z longitudinal (along the beam direction). The positive polarization directions ($\uparrow$) are defined with respect to a right-handed coordinate frame fixed in the laboratory in which the x axis is horizontally to the left looking downstream, the y axis is upward in the laboratory, and the z axis is along the beam direction. Since A_i^{coinc} involves measurements of relative double differential cross sections, they can be written as

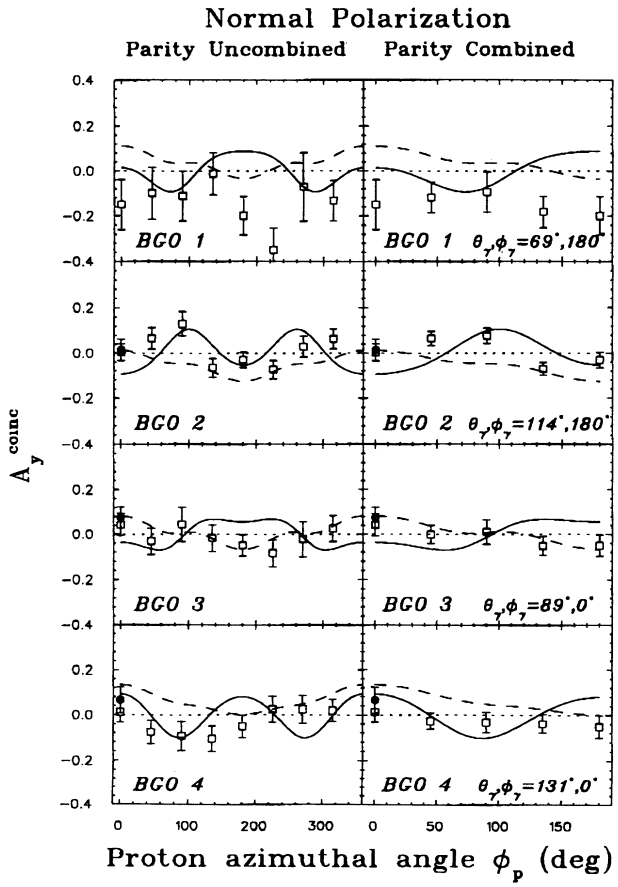

FIG. 10. A_y^{coinc} vs ϕ_p for normal polarization data. The solid lines are DREX and the dashed lines are DW81. The solid points are data from Hicks *et al.* [9].

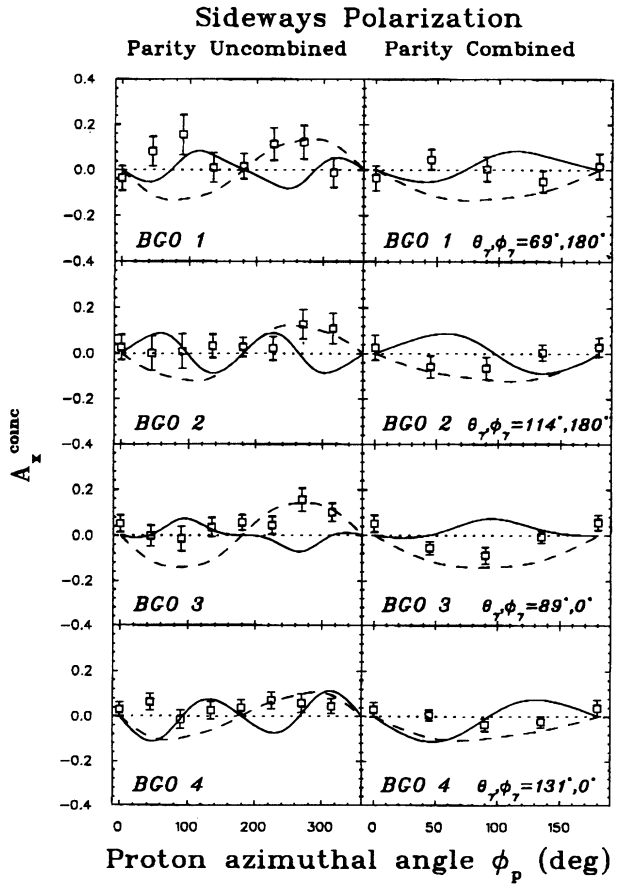

FIG. 11. A_x^{coinc} vs ϕ_p for sideways polarization data. The solid lines are DREX and the dashed lines are DW81.

$$A_i^{\text{coinc}}(\phi_p,\theta_\gamma,\phi_\gamma)=\frac{1}{P}\left(\frac{H_\uparrow-QH_\downarrow}{H_\uparrow+QH_\downarrow}\right),$$

where $H_\uparrow$ and $H_\downarrow$ are the measured BGO spectrum peak amplitudes and Q is the ratio of average beam charge $\uparrow$ to $\downarrow$ described in the preceding section. Measured values for $A_i^{\text{coinc}}(\phi_p,\theta_\gamma,\phi_\gamma)$ are presented in Figs. 10, 11, and 12.

The slow variation with proton azimuthal scattering angle and geometric symmetries provide several constraints on the data. These constraints permit combining data for improved statistics.

(a) Due to the low multipolarity ($j=1$) of the radiation, data for three adjacent S2 sectors were combined (Fig. 2), giving an average azimuthal bin size of 68°. Since points in Figs. 10, 11, and 12 are separated by 45°, there is some overlap of data between adjacent points, i.e., one of the 22.5° angle elements is common to each pair of neighboring points.

(b) Overall reaction parity and rotational invariance were utilized to additionally combine data points and estimate systematic errors. In the case of normal beam polarization, parity conservation requires that the analyzing-power measurements be symmetric about $\phi_p=180°$. Data for corresponding S2 sectors were added:

$$A_i^{\text{coinc}}(\phi_p,\theta_\gamma,\phi_\gamma)$$

$$=\frac{1}{P}\left(\frac{(H_{1\uparrow}-QH_{1\downarrow})+(H_{2\uparrow}-QH_{2\downarrow})}{(H_{1\uparrow}+QH_{1\downarrow})+(H_{2\uparrow}+QH_{2\downarrow})}\right),$$

where 1 refers to the peak amplitudes for ϕ_{p1} with $0°<\phi_{p1}<180°$ and 2 refers to amplitudes for the direction $\phi_{p2}=360°-\phi_{p1}$. These results are shown in the right-hand side of Fig. 10. For sideways and longitudinal polarization cases, the A_i^{coinc} should be antisymmetric about $\phi_p=180°$, and data for corresponding sectors were subtracted:

$$A_i^{\text{coinc}}(\phi_p,\theta_\gamma,\phi_\gamma)$$

$$=\frac{1}{P}\left(\frac{(H_{1\uparrow}-QH_{1\downarrow})-(H_{2\uparrow}-QH_{2\downarrow})}{(H_{1\uparrow}+QH_{1\downarrow})+(H_{2\uparrow}+QH_{2\downarrow})}\right),$$

where 1 and 2 have the same meaning as before (right-hand sides of Figs. 11 and 12).

To evaluate the systematic error determined by the parity constraints, the distribution of differences (or sums) of pairs of analyzing powers that should equal zero was examined. For normal beam polarization for each BGO the differences were $A(\phi_p=45°)-A(\phi_p=315°)$, $A(\phi_p=90°)-A(\phi_p=270°)$, and $A(\phi_p=135°)-A(\phi_p=225°)$. [Parity invariance makes no prediction about $A(\phi_p=0°)$ and $A(\phi_p=180°)$.] For sideways and longitudinal polarization, the sums were $A(\phi_p=45°)+A(\phi_p=315°)$, $A(\phi_p=90°)+A(\phi_p=270°)$, and $A(\phi_p=135°)+A(\phi_p=225°)$. $A(\phi_p=0°)$ and $A(\phi_p=180°)$ were individually included. The errors for these combinations were obtained from the statistical errors of the analyzing powers (Sec. III). The resulting distribution in units of the standard deviations is shown in Fig. 13. The mean of this distribution is 0.33 ± 0.15, i.e., approximately one-third of the statistical errors given can additionally arise from systematic errors. The standard deviation from zero of the distribution, i.e., the root mean square of the deviations from zero, is 1.23 ± 0.15, which is slightly more than the expected value of 1.0. Out of a total of forty-seven measurements, 53.2% are 1σ or more away from zero, which

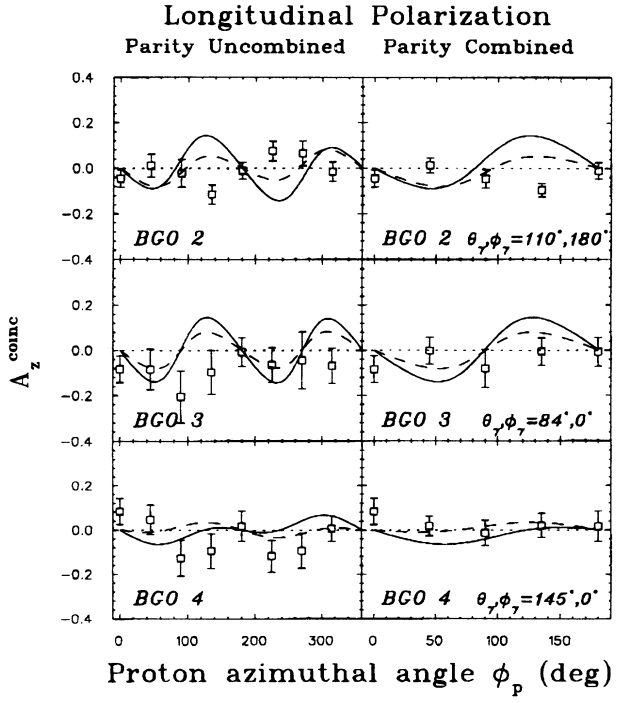

FIG. 12. A_z^{coinc} vs ϕ_p for longitudinal polarization data. The solid lines are DREX and the dashed lines are DW81.

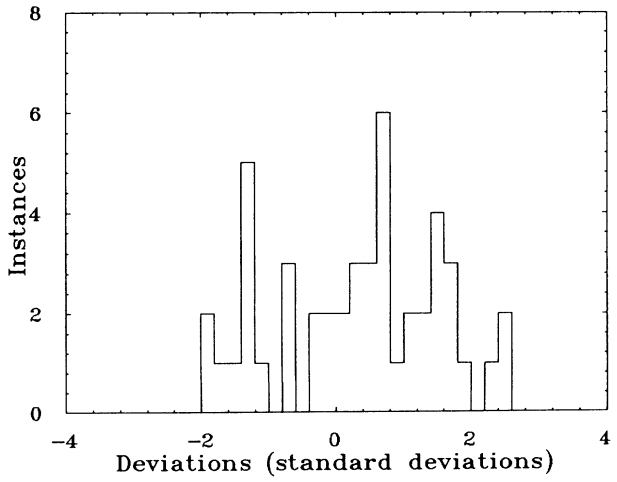

FIG. 13. Distribution of combinations of the analyzing powers that should equal zero by parity considerations for all directions of polarization, divided by their standard deviations.

is more than can be expected from statistics alone. (If this quantity were normally distributed we would expect only 32% to be more than 1σ from zero.) Thus there is indication that some systematic error is present and that the error bars shown in Figs. 10, 11, and 12 are only about 80% of the true error bars ($\sigma_{\text{actual}} = 1.23\sigma_{\text{stat}}$).

(c) Two other symmetries were used to combine data points from BGO's 1 and 2 to further improve statistics. The result is called BGO A and is seen in the top part of Fig. 14. (BGO's 3 and 4 are the same as in Figs. 10 and 11, and are included in Fig. 14 for comparison as discussed below.) Rotational invariance about the z axis results in the analyzing power for BGO 1 at $\phi_p = a$ being equal in magnitude but opposite in sign to the analyzing power at $\phi_p = a + 180°$ for a BGO position reflected through the x-y plane; i.e.,

$$A^{\text{coinc}}(\phi_p = a, \theta_\gamma = 69°, \phi_\gamma = 180°) = -A^{\text{coinc}}(\phi_p = a + 180°, \theta_\gamma = 69°, \phi_\gamma = 0°). \quad (3)$$

A second symmetry (parity in the γ decay, Ref. [7], Eq. (4.10)) requires that the measured asymmetry be the same for γ-ray detectors at diametrically opposed p-^{12}C center-of-mass angles, and so

$$A^{\text{coinc}}(\phi_p = a + 180°, \theta_\gamma = 69°, \phi_\gamma = 0°) = A^{\text{coinc}}(\phi_p = a + 180°, \theta_\gamma = 117°, \phi_\gamma = 180°). \quad (4)$$

Combining Eqs. (3) and (4) gives

$$A^{\text{coinc}}(\phi_p = a, \theta_\gamma = 69°, \phi_\gamma = 180°) = -A^{\text{coinc}}(\phi_p = a + 180°, \theta_\gamma = 117°, \phi_\gamma = 180°). \quad (5)$$

The BGO position for the right-hand side of Eq. (5) is only 6° from BGO 2 at $\theta_\gamma, \phi_\gamma = 117°, 180°$, which is small compared to the 20° acceptance of each BGO, and hence this relationship has been used in Fig. 14 to combine points from BGO's 1 and 2 into BGO A at the mean θ_γ value of 114°.

With the S2 scintillator sectors defining proton scattering angles between 3.3° and 11.2° (Sec. III), the average cross-section-weighted (center-of-mass) polar angle for our data is 7.3°. The data show small analyzing powers, less than 0.10, with error bars of the same order. The agreement is good between our data and data from Hicks *et al.* [9] for normally polarized 400-MeV protons scattered to (center-of-mass) polar angles of $\theta_p = 6.7°$, shown as solid dots in Figs. 10 and 14.

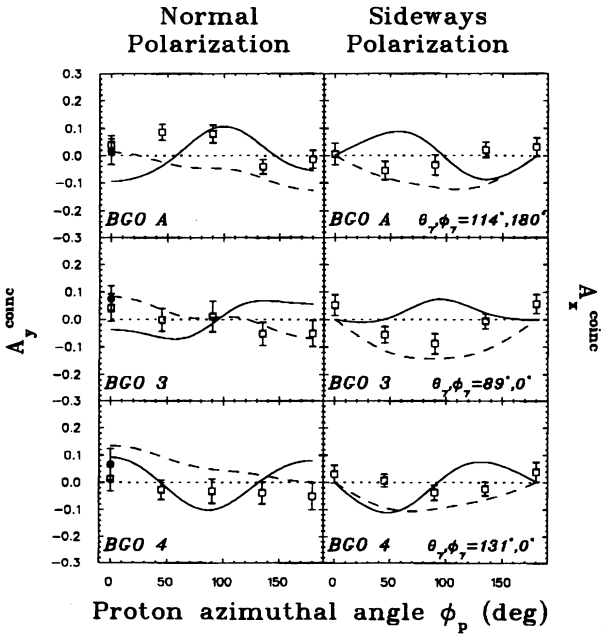

FIG. 14. $A_{y,x}^{\text{coinc}}$ for BGO's 1 and 2 have been combined into BGO A as described in the text. BGO's 3 and 4 are the same as in Figs. 10 and 11, reproduced here to aid in seeing any trends.

Predictions of a nonrelativistic distorted-wave calculation DW81 [14] (dashed line), and a relativistic treatment with explicit exchange DREX [5] (solid line) using (p,p') spin amplitudes for 400-MeV incident proton energy are also shown in Figs. 10, 11, 12, and 14. The amplitudes and the program to calculate the γ-ray coincidence analyzing powers from them were provided by Piekarewicz [15]. The calculated analyzing powers were averaged by the authors over the same BGO and proton arm solid angles for which the data are presented. The nonrelativistic calculation DW81 uses the Love-Franey NN interaction, and distorted waves from an optical potential derived from the 400-MeV data of Jones *et al.* [16]. The relativistic calculation DREX, which handles exchange between the projectile and target nucleons explicitly, uses the NN interaction of Horowitz [17], and distorted waves from a $t\rho$ optical potential using this NN interaction and a nucleon density determined from electron scattering. Both NN interactions are fit to the same Arndt phase shifts [18], and both calculations use Lee and Kurath nuclear wave functions [19].

In general, the magnitudes of the measured analyzing powers are somewhat less than those predicted by both relativistic and nonrelativistic models, and yet also consistent with zero. The overall (all three directions of polarization) root-mean-square asymmetry for our data was 0.050±0.007; for DREX predictions at the same points it is 0.063, and for DW81 at those points it is 0.065. The longitudinal results in Fig. 12 show some indication of being opposite in sign or out of phase with both predictions. The plots have been arranged in Fig. 14 so that they are in vertically descending θ_γ order, in order to show trends in both the data and the predictions as θ_γ changes. (BGO A of normal and sideways polarizations at $\theta_\gamma, \phi_\gamma = 114°, 180°$ is equivalent to one at $\theta_\gamma, \phi_\gamma = 66°, 0°$ because of the third symmetry mentioned above, and BGO 2 of longitudinal polarization

with $\theta_\gamma, \phi_\gamma = 110°, 180°$ is equivalent for the same reason to $\theta_\gamma, \phi_\gamma = 70°, 0°$.)

In summary, it is seen that the data do not follow the predictions, and neither model is clearly confirmed by the data.

ACKNOWLEDGMENTS

This work was supported in part by the National Science Foundation, with Grants No. PHY85-09880 and No. PHY88-11792, the National Aeronautics and Space Administration, with Grant No. NAG-1-416, and the U.S. Department of Energy. We wish to thank Jorge Piekarewicz for supplying the amplitudes and help in computing the theoretical predictions. Appreciation and thanks also go to John Bensel and Melvin Woods at the William and Mary machine shop for their work in constructing S1 and S2. Finally, we would like to thank Mike McNaughton at LAMPF for all his help with the experiment.

[1] J.R. Shepard, J.A. McNeil, and S.J. Wallace, Phys. Rev. Lett. **50**, 1443 (1983).

[2] K.H. Hicks, R.G. Jeppesen, C.C.K. Lin, R. Abegg, K.P. Jackson, O. Häusser, J. Lisantti, C.A. Miller, E. Rost, R. Sawafta, M.C. Vetterli, and S. Yen, Phys. Rev. C **38**, 229 (1988).

[3] D. Frekers, S.S.M. Wong, R.E. Azuma, T.E. Drake, J.D. King, L. Buchmann, R. Schubank, R. Abegg, K.P. Jackson, C.A. Miller, S. Yen, W.P. Alford, R.L. Helmer, C. Broude, S. Mattsson, and E. Rost, Phys. Rev. C **35**, 2236 (1987).

[4] J.R. Comfort, G.L. Moake, C.C. Foster, P. Schwandt, and W.G. Love, Phys. Rev. C **26**, 1800 (1982).

[5] E. Rost and J.R. Shepard, Phys. Rev. C **35**, 681 (1987).

[6] K.H. Hicks, O. Häusser, R. Abegg, W.P. Alford, A. Celler, R.L. Helmer, R.S. Henderson, K.P. Jackson, J. Lisantti, C.A. Miller, R. Sawafta, J.R. Shepard, and S. Yen, Phys. Lett. B **201**, 29 (1988).

[7] J. Piekarewicz, E. Rost, and J.R. Shepard, Phys. Rev. C **41**, 2277 (1990).

[8] K.H. Hicks, R. Abegg, A. Celler, O. Häusser, R.S. Henderson, N.W. Hill, K.P. Jackson, R.G. Jeppesen, N.S.P. King, M.A. Kovash, R. Liljestrand, C.A. Miller, G.L. Morgan, J.R. Shepard, A. Trudel, M. Vetterli, and S. Yen, Phys. Rev. Lett. **61**, 1174 (1988).

[9] K.H. Hicks, in *Spin Observables of Nuclear Probes*, edited by C. Horowitz, C. Goodman, and G. Walker (Plenum, New York, 1988), p. 111.

[10] P. Schwaller, B. Favier, D.F. Measday, M. Pepin, P.U. Renberg, and C. Serre, CERN Report CERN 72-13, 1972.

[11] O.B. van Dyck, private communication.

[12] W.R. Nelson, H. Hirayama, and D.W. Rogers, SLAC Report SLAC-265, UC-32, 1985.

[13] R. Brun, I. Ivanchenko, and P. Palazzi, HBOOK Users Guide, Data Handling Division, CERN. HFIT is a modified form of the fitting program from MINUIT, by F. James and M. Roos.

[14] Program DWBA70, R. Schaeffer and J. Raynal (unpublished); extended version DW81, J.R. Comfort (unpublished).

[15] Jorge Piekarewicz, private communication.

[16] K. Jones, C. Glashausser, R. de Swiniarski, S. Nanda, T.A. Carey, W. Cornelius, J.M. Moss, J.B. McClelland, J.R. Comfort, J.-L. Escudie, M. Gazzaly, N. Hintz, G. Igo, M. Haji-Saeid, and C.A. Whitten, Jr., Phys. Rev. C **33**, 17 (1986).

[17] C.J. Horowitz, Phys. Rev. C **31**, 1340 (1985).

[18] R.A. Arndt and L.S. Roper, code SAID, 1984 (unpublished).

[19] T.-S.H. Lee and D. Kurath, Phys. Rev. C **21**, 293 (1980).